THE ASTROPHYSICAL JOURNAL, Vol. 151, January 1968

SKY SURVEY OF HIGH-ENERGY COSMIC X-RAYS AND SPECTRA OF THE SOURCES IN THE CRAB NEBULA AND CYGNUS*

G. W. CLARK, W. H. G. LEWIN, AND W. B. SMITH
Laboratory for Nuclear Science and Department of Physics
Massachusetts Institute of Technology

Received June 16, 1967

ABSTRACT

The northern sky from right ascension 19^h to 7^h and declination $-10°$ to $+75°$ was surveyed on July 19, 1966, for X-ray sources above 20 keV in a single flight with a balloon-borne detector having a sensitive area of 368 cm², a 12° FWHM field of view, and a direction determination accuracy of ±2° Two intensity peaks were observed, each with a signal-to-noise ratio greater than 25 to 1. One was identified with Tau X-1 (the Crab Nebula), and the other with Cyg X-1 and/or Cyg X-3. The spectral data of the two peaks were similar in the observed range between 20 and 100 keV and could be described in terms of incident spectra in the form of $dN/dE \sim E^{-(1+\alpha)}$ with $\alpha = 0.6 \pm 0\,2$, as well as in the form of $(1/E)$ $\exp(-E/kT)$ with $kT = 60 \pm 20$ keV The intensity ratio of the two peaks was Cyg/Tau X-1 = 0 84 ± 0.10 in the energy range from 20 to 70 keV No other intensity peak greater than one-eighth that of Tau X-1 was found in the region of sky surveyed and more than 10° away from the centers of both the Taurus and Cygnus peaks. This region includes the blue, starlike X-ray source Cyg X-2, the supernova remnants Cas A and Cas B (Tycho's SN_1), the Andromeda galaxy M31 and the radio sources 3C 403, 3C 446, CTA 102, 3C 93, 3C 9, 3C 47, 3C 147. Since Cyg X-2 has an intensity at 3 keV comparable to that of the combined intnsities of Cyg X-1 and Cyg X-3 in rocket observations at 3 keV, but was not discernible at 30 keV, it has a significantly steeper spectrum than Cyg X-1 and Tau X-1 from 3 to 30 keV as does Sco X-1, which has a similar optical appearance.

I. INTRODUCTION

A previous balloon experiment of this laboratory (Clark 1965) carried out in July, 1964, extended the measurements of the X-ray spectrum of Tau X-1 (the Crab Nebula) into the energy range above 20 keV. Since then other groups have reported observations of several X-ray sources above 20 keV, including Tau X-1 (Peterson, Jacobson, and Pelling 1966; Haymes and Craddock 1966; Grader, Hill, Seward, and Toor 1966), Cygnus (McCracken 1966; Grader *et al.* 1966; Boldt, McDonald, Riegler, and Serlemitsos 1966; Brini, Ciriegi, Fuligni, Moretti, and Vespignana 1967; Bleeker, Burger, Deerenberg, Scheepmaker, Swanenburg, and Tanaka 1967), Sco X-1 (Peterson and Jacobson 1966), as well as the diffuse component of cosmic X-radiation (Rocchia, Rothenflug, Boclet, Ducros, and Labeyrie 1966).

The objectives of the present experiment were to observe the sources in Taurus and Cygnus during a single flight with a periodically calibrated and stable detector having a high signal-to-noise ratio, and to search for high-energy X-rays from the weaker known sources as well as from other sources which may have escaped detection so far. We used a detector with a sensitive area four times larger than the one in the previous experiment, and with a more effective system of shielding to suppress background counts. These improvements, together with others in the orientation determination and data recording and processing systems resulted in a large improvement in sensitivity and accuracy.

We report here the results from a general survey of the northern sky from right ascension 19^h to 7^h and declination $-10°$ to $+75°$ carried out in a single flight on July 19, 1966. Spectral data from 20 to 100 keV for the sources in the Crab Nebula and in the constellation Cygnus are presented together with upper limits on the intensities of Cyg X-2, Cas A, Cas B, M31 and several quasi-stellar sources (QSS).

* Supported in part by the National Aeronautics and Space Administration under Grant NsG-386 and in part by the U S Atomic Energy Commission under contract AT(30-1)2098.

II. INSTRUMENTATION

The instrument had four scintillation X-ray detectors surrounded on the bottom and sides by a graded radiation shield of lead and tin inside of a plastic scintillator anticoincidence shield as shown in Figure 1. Each detector was a NaI (Tl) crystal 1 mm thick and 92 cm^2 in effective area optically coupled to a 5-inch photomultiplier by a cylindrical lucite light pipe.

The field of view was defined by a square honeycomb collimator of $\frac{1}{32}$-inch brass slats which gave the detector an angular response that can be represented by the product of two triangular functions as follows:

$$A(\theta_x,\theta_y) = A_0\left(1-\frac{|\theta_x|}{\theta_0}\right)\left(1-\frac{|\theta_y|}{\theta_0}\right), \qquad |\theta_x| < \theta_0,\ |\theta_y| < \theta_0$$

$$= 0, \qquad |\theta_x| > \theta_0,\ |\theta_y| > \theta_0,$$

where $A(\theta_x,\theta_y)$ is the projected exposed area of the crystals for an incidence direction whose angles with respect to the two sets of perpendicular collimator planes are θ_x and θ_y. The constants are $A_0 = 368$ cm^2 and $\theta_0 = 12°$.

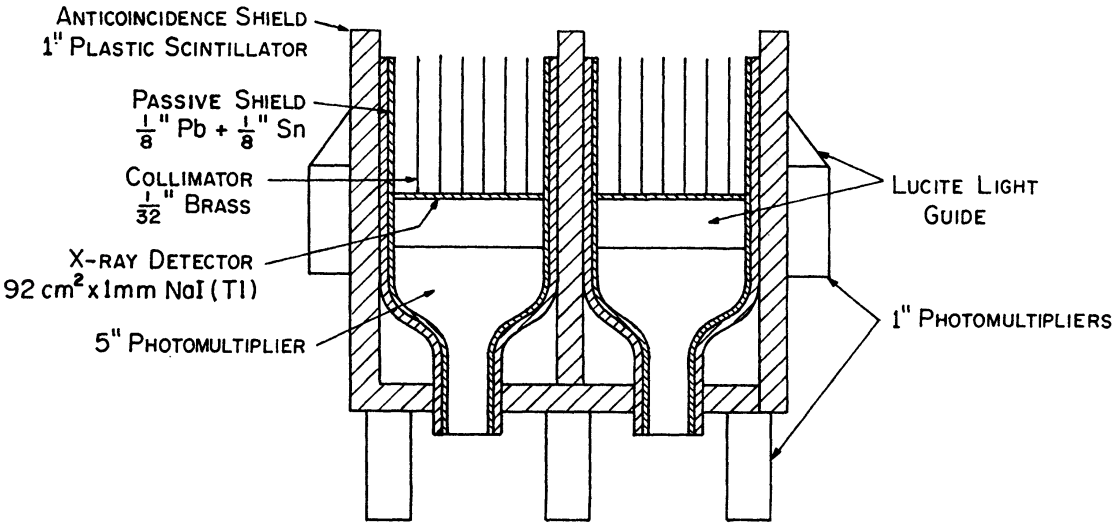

FIG. 1.—Schematic diagram of the detector

The pulses from the detectors were added and analyzed by a five-channel pulse-height analyzer whose outputs were fed to five scalers. The scalers were connected to display lights in a photographic data box and were recorded as dashed trails on a steadily moving film. The added pulses from the nine phototubes attached to the plastic scintillator were connected in anticoincidence with the detectors. Periodic interruption of the anticoincidence logic during the flight demonstrated that the anticoincidence shield functioned properly throughout the flight, and suppressed the background counting rate by a factor of 2.6 in channels 1–4 and by a factor of 4 in channel 5. The channels of the pulse-height analyzer were set with reference to the energy spectra of the radioactive sources Am^{241} (16.5 and 59.6 keV) and Sn^{119} (~25 keV). The channel settings before flight were approximately 10–20, 20–35, 35–48, 48–70, >70 keV. Periodic exposure of a radioactive source of Am^{241} mounted in front of the detector provided calibration data from which we determined every 10 min the values of the channel settings throughout the flight.

The time base for the data record was provided by a tuning-fork oscillator whose scaled outputs of 1 and 10 sec controlled two of the display lights. Another display light was connected to a sun sensor. Azimuthal orientation data were obtained from two crossed flux-gate magnetometers mounted in a horizontal plane. The magnetometer outputs were continuously registered on the film. A barometer, a clock and a thermometer were photographed every 30 sec.

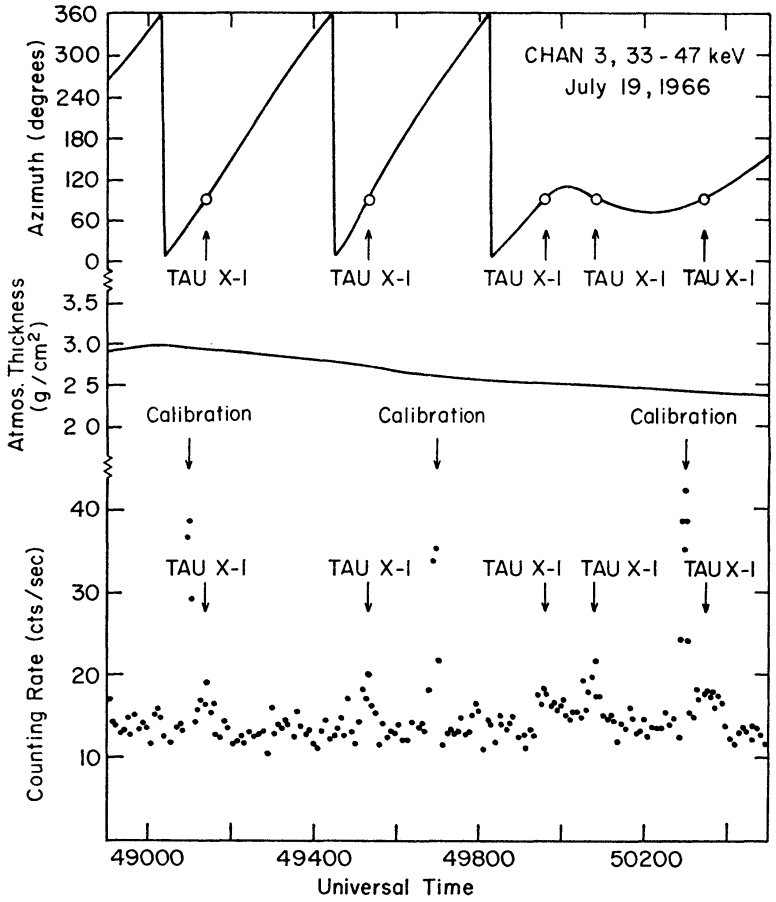

FIG. 2.—Portion of data recorded when Tau X-1 was observed. *From top to bottom*: Azimuth of the detector axis; atmospheric pressure at float altitude; counting rate in channel 3.

The apparatus was suspended with the detector axis inclined at 40° from the vertical. A line rotator with a period of 7 min turned the instrument in azimuth. The flight was carried by a 10.6 million cubic foot balloon that was launched from Palestine, Texas, and floated above 133000 feet from 0810 hours till cutdown at 1600 hours U.T. Figure 2 shows a portion of the flight record.

III. DATA ANALYSIS AND RESULTS

a) Survey Map and Source Locations

We consider first the location and spectra of the discrete high-energy X-ray sources that are discernible in our data. As the instrument rotated about the vertical, its field of view swept out an annulus of directions with a mean zenith angle of 40°. As the flight progressed, the diurnal motion carried this annulus across the celestial sphere in right ascension, thereby providing a general survey of the region of the sky within the bound-

ary line shown in Figure 3. The total time during which various celestial directions within the surveyed region were within the field of view varied, due to the systematic effect which favors those directions near the extreme north and south boundaries where the diurnal motion is nearly tangent to the circle described by the detector axis, as well as due to changes in the angular velocity of rotation caused by rotations of the balloon. Thus the lower limit on the detectable intensity of sources within the surveyed region varies according to direction, and the absence of a detectable source in a given direction must be interpreted according to the total local exposure.

Changes in the counting rates due to the two discrete sources in Taurus and Cygnus were immediately discernible on plots of the rates in channels 2, 3, and 4 versus time as shown for the case of Tau X-1 (channel 3) in Figure 2. Since there was no doubt about the identification of Tau X-1 as the cause of the counting-rate peaks observed between 48000 and 52000 sec U.T., we used these peaks to check the direction determination which was based on a preflight calibration of the magnetometers, taking into account the magnetic deviation during the flight. Agreement was found within 2°.

We analyzed the counting rate and orientation data from the entire flight to obtain a general X-ray survey map of the sky in the region within the boundary shown in Figure 3. This map shows the combined data from channels 2, 3, and 4 which cover the range of X-ray energies from 20 to 70 keV. To obtain this map we first tabulated the counts and exposure time versus celestial direction for each of the channels. For these tabulations we assigned a computer register for "total counts" and another for "exposure time" to each element of solid angle in a two-dimensional array of elements defined by 5° intervals of declination and $5°/\cos\delta$ intervals of right ascension, where δ is the center value of the declination interval. Using the digitized magnetometer data derived from the film record we determined the celestial direction of the detector axis at the midpoint of the time interval of each 64-count cycle, and then added the duration of interval and 64 counts, respectively, to the "exposure time" and "total counts" registers corresponding to the solid angle element within which this direction was located. At the end of the tabulation we computed the average rate for each solid angle interval. This procedure was repeated for each channel. The average r and its standard deviation ρ for channels 2, 3, and 4 combined were then calculated from the formula

$$r \pm \sigma = \sum_{i=2}^{4} \frac{N_i}{t_i} \pm \sqrt{\sum_{i=1}^{4} \frac{N_i}{t_i^2}},$$

where N_i and t_i are the accumulated counts and exposure time in a given register for the ith channel.

The map shows the solid angle elements whose average intensities were greater than the over-all average obtained by dividing the total number of counts recorded during the entire period of observation in channels 2, 3, and 4 by the total effective exposure time. The latter was defined to be the sum of the effective exposure times for each solid angle element which we calculated by dividing the number of counts, ΣN_i, for the element by the combined average r calculated according to equation (1). The number of vertical bars in each square solid angle element in Figure 3 denotes the number of standard deviations by which the intensity is above the over-all average.

The two clusters of solid angle elements with above-average intensities, which stand out clearly on the sky map, contain the positions previously reported for Tau X-1 and Cyg X-1. No other separate clusters of above-average elements can be discerned, and from this fact we conclude that no other source with an intensity larger than one-eighth that of Tau X-1 in the spectral range from 20 to 70 keV and separated from Cyg X-1 and Tau X-1 by 10° or more existed in this region at the time of our survey. More precise limits on the possible intensity of several specific objects relative to the Taurus and Cygnus sources can be derived from the raw counting rate data given in Table 1.

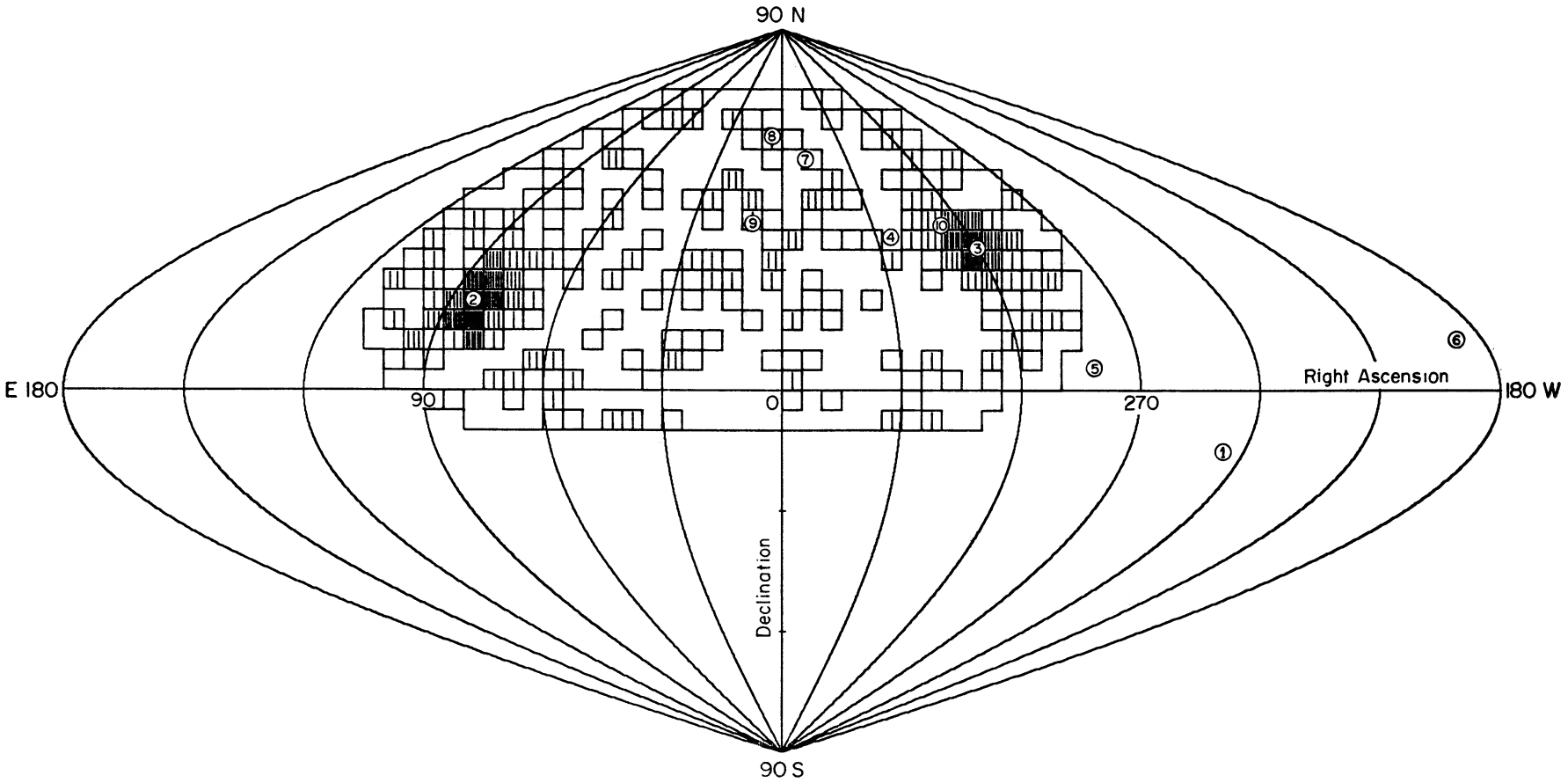

FIG. 3.—Sky map (20–70 keV) showing the area scanned (from July 19, 1966, balloon flight). The number of vertical bars in each 5° × 5° box represents the number of standard deviations by which the observed counting rate exceeds the average. No bar means zero to 1 standard deviation; one bar means 1–2 standard deviations, etc. Since the exposure of different parts of the sky was not uniform, the number of bars presented in one box is not strictly proportional to the intensity. The identifications of the numbered objects are as below:

Object	R.A.	Decl.	Object	R.A.	Decl.	Object	R.A.	Decl.
(1) Sco X-1	244.8	−15.5	(5) Ser XR-1	281.3	5.3	(8) Cas B	5.8	63.9
(2) Tau X-1	82.9	22.0	(6) Vir A	187.0	12.7	(9) M31	10.0	41.0
(3) Cyg X-1	299.3	35.1	(7) Cas A	350.3	58.5	(10) Cyg X-3	307.7	40.9
(4) Cyg X-2	325.6	37.2						

We computed the position of the center of the second cluster of above-average intensities near right ascension 300° in the constellation Cygnus under the assumption that it was due to a single source, and found $\alpha = 300° \pm 2°$ and $\delta = 35° \pm 2°$. This is consistent with the precise position $\alpha = 19^h56^m34^s$, $\delta = 36°6'$ of Cyg X-1 obtained from rocket data by Giacconi, Gorenstein, Gursky, and Waters (1967). They also reported a source, Cyg X-3, of intensity about one-third of Cyg X-1 lying about 10° away. In an attempt to determine whether one or the other or both of these sources cause the peak in our Cygnus data, we plotted the intensities (20–70 keV) versus the relative angle between telescope axis and the directions of the sources Tau X-1 and Cygnus X-1 as presented in Figure 4. The Cygnus plot is evidently consistent with the Cygnus source's being a single concentrated one like Tau X-1. On the other hand, calculations show that

TABLE 1

COUNTING RATES ABOVE BACKGROUND (counts/368 cm²) OBSERVED IN DIRECTIONS OF VARIOUS OBJECTS CORRECTED TO ATMOSPHERIC THICKNESS OF 2.5 SECANT 40° gm cm^{-2}*

OBJECT	CHANNEL NUMBER AND NOMINAL CHANNEL BOUNDARIES (IN KEV)				
	1 (10–20)	2 (20–34)	3 (34–47)	4 (47–70)	5 (> 70)
Tau X-1	+3 87±0 5	+6 58±0 5	+6 13±0 4	+7 80±0 5	+5.44±1 0
Cyg X-1/X-3	+0 87± 5	+5 34± .6	+5 87± .4	+6 10± 6	+7.11±1 2
Cyg X-2	−0 2 ± .6	+0 3 ± .6	+0 7 ± .6	+0 8 ± 7	−1 5 ±1 8
Cas A	−0 3 ± .5	0 0 ± 6	+0 7 ± 4	+0 0 ± .5	+0 8 ±1 5
Cas B	+0 4 ± .4	+0 4 ± .4	−0 3 ± .2	−0 2 ± .4	+2 8 ±1 2
M31	+1 3 ± 6	−1.6 ± .7	−0 8 ± .5	−0 7 ± .7	+2.4 ±1 7
3C 403	−1 1 ± .7	−1 5 ± .8	−1 2 ± .5	−0 6 ± .7	−2 3 ±2 0
3C 446	−0 2 ± 4	−0 9 ± .4	−0 9 ± 3	+0 4 ± .4	−2 4 ±1 4
CTA 102	−0.2 ± .5	−0 5 ± .5	−0 4 ± 4	−0 1 ± .5	−2 5 ±1 5
3C 93	−0 1 ± .5	+0 3 ± 6	+0 5 ± .4	−0 1 ± .4	−1 2 ±1.4
3C 48	+1 3 ± .6	−0 4 ± .6	−0 5 ± .5	−0.5 ± .5	+3 0 ±1.5
3C 9	0 0 ± .5	−0 1 ± 6	−0 6 ± .5	−1.8 ± .6	+1.4 ±1 5
3C 47	+1 3 ± 6	+1 3 ± 7	+0 3 ± .5	+0 1 ± 6	...
3C 147	+1.6 ±0.6	+1 5 ±0 7	−0.4 ±0 5	−0 2 ±0 6	...

* No corrections have been made for the detector response, energy resolution, or K escape, etc. Indicated uncertainties are estimated standard deviations due to counting statistics and uncertainties in the evaluations of background rates.

this test is fairly insensitive to the existence of another source within the angular resolution of the detector. We also made two-dimensional plots of the intensities (20–70 keV) in 4° × 4° elements around the position of Cyg X-1 and, for comparison purposes, of Tau X-1 as shown in Figure 5. These plots indicate that the Cygnus peak is somewhat more spread out than that of the single source Tau X-1 and that it may therefore contain significant contributions from Cyg X-3. Although the angular resolution of this observation is evidently not sufficient to determine the relative magnitudes of the contributions, from Cyg X-1 and Cyg X-3 the results do suggest that Cyg X-1 is predominant.

b) Spectra of Tau X-1 and Cyg X-1/X-3

We consider next the analysis of the spectral data of the two peaks. The first step was the evaluation of the counting rates for the various pulse-size channels at the average altitude of observation due to the source when it was in the center of the field of view. The experimental data consist of the durations Δt_i of successive time intervals in each of which a preset number of counts is recorded, together with the atmospheric depths and celestial orientations of the instrument at the midpoints of these intervals. Calling θ_{xi} and θ_{yi} the angular coordinates of the source with respect to the center of the field of

view at the midpoint of the ith interval, and x_i the atmospheric depth, we define the effective exposure W (area × time) for a given source by the relation

$$W = \sum_i A_0 f(\theta_{xi}, \theta_{yi}) \Delta t_i \exp[-(x_i - x_0)/\lambda],$$

where A_0 is the sensitive area of the detector, $f(\theta_1)$ is the angular response function of the detector, x_0 is the average atmospheric depth during the observation, and λ is the

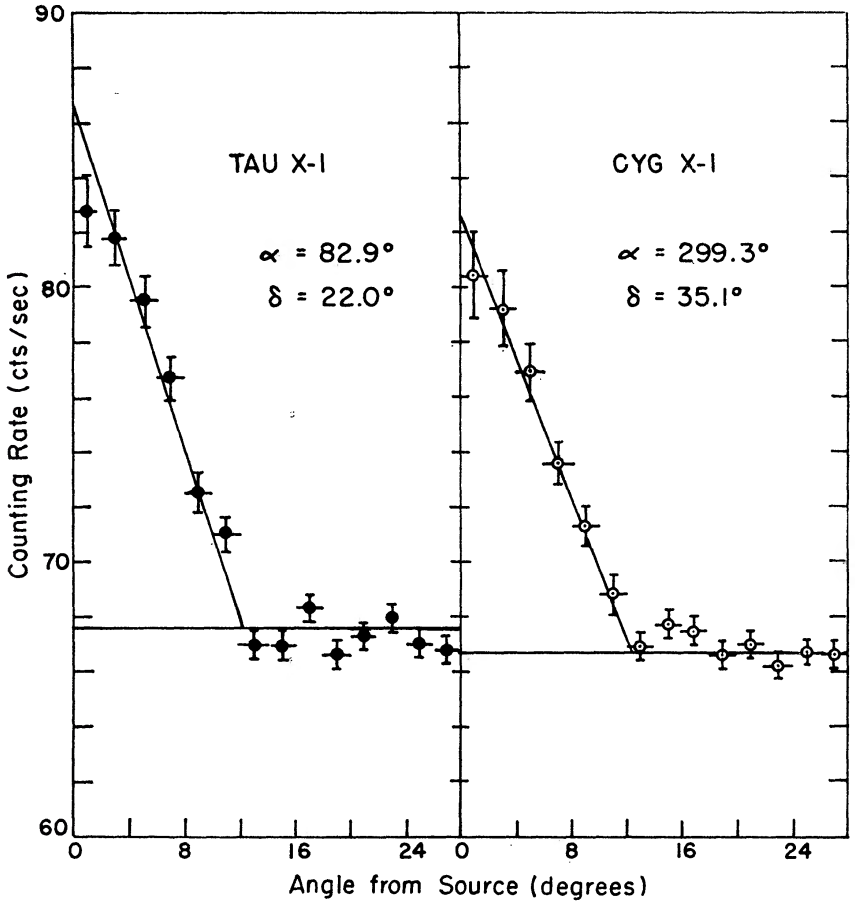

FIG. 4.—Plots of counting rates (20–70 keV) versus angle between the detector axis and the directions of Tau X-1 and Cygnus X-1. The slant lines are the theoretical response curves of the detector which intersect the background rate at 12°.

effective absorption length for the primary radiation detected in the given channel. We call N the total number of counts that occurred during all of the intervals Δt_i, and denote by $\langle B \rangle$ the average background counting rate per unit area at depth x_0. The counting rate per unit area is now defined by the equation

$$S(x_0) = \frac{(N - \langle B \rangle \Sigma \Delta t_i)}{\Sigma A f(\theta_{xi}, \theta_{yi}) \Delta t_i \exp[-(x_i - x_0)/\lambda]}.$$

For simplicity in the calculations we replaced the function $f(\theta_x, \theta_y)$ by the adequate approximation

$$f = (1 - \theta/\theta_0), \qquad \theta \leq \theta_0$$
$$= 0 \qquad , \qquad \theta > \theta_0,$$

where

$$\theta = \sqrt{(\theta_x^2 + \theta_y^2)}, \qquad \theta_0 = 12^\circ.$$

To optimize the statistical accuracy in the determination of $s(x_0)$ for a given source, we included only those intervals when the source was within an angle less than 8° from the center of the field of view. The results for the two sources in the five energy channels are shown in Figure 6. The errors in the "data points" are mainly due to counting-rate statistics.

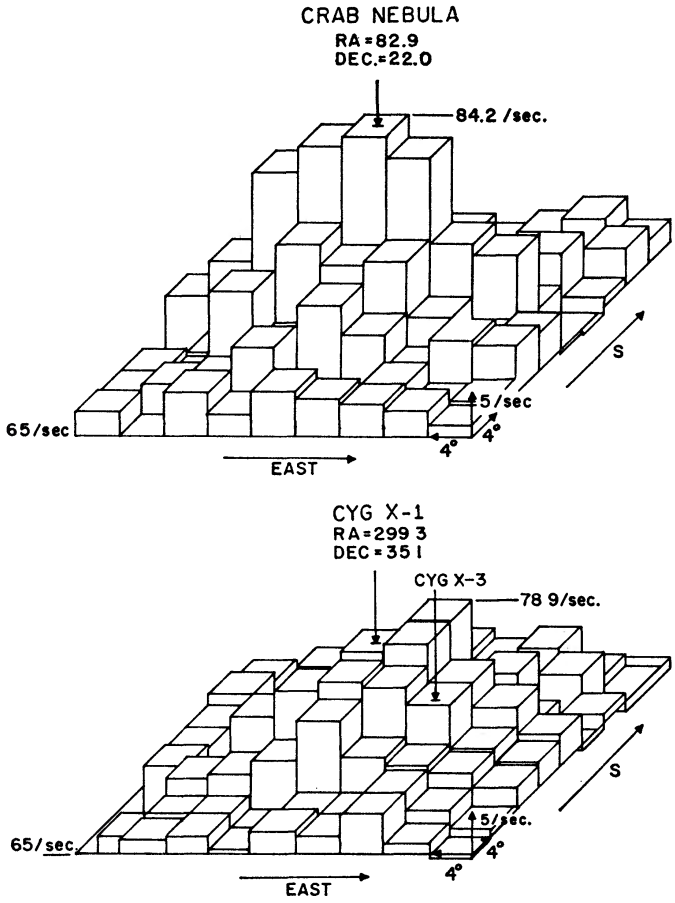

FIG. 5.—Three-dimensional plots of the counting rate (20–70 keV) versus direction for the region around Tau X-1 and around Cyg X-1 and Cyg X-3 through 3.3 gm/cm² of air.

The second step in our spectrum analysis was to represent the unknown primary differential number spectrum by a plausible function with adjustable parameters and to determine the values of these parameters for which the predicted counting rates at the level of observation matched those observed. Calling this function $N(E)$, where E is the X-ray photon energy, we calculated the quantities

$$S_j(x_0) = \int_0^\infty dE \int_{h_j-}^{h_j+} N(E)\, t(E,X_0)\, U(E)\, e^{-\mu(E)x_0}\, g(E,h)\, dh,$$

where $S_j(x_0)$ is the expected rate per unit area in the jth channel, $t(E,x_0)$ is the transmission of the air and the material over the detector for X-rays of energy E, $U(E)$ is the

detection efficiency of the NaI (Tl) crystal, $g(E,h)dh$ is the probability that an X-ray of energy E incident on the detector will produce a pulse of height h in dh, and h_j^- and h_j^+ are the lower and upper bounds of the jth pulse-height channel. The function $g(E,h)$ takes the phenomenon of K X-ray escape into account (Stein and Lewin 1967) and approximates the spread in size of pulses produced by a given energy release E in the crystal by a Gaussian with a standard deviation given by

$$\sigma(E) = (0.10E + 0.46\sqrt{E}) \ (E \text{ and } \sigma \text{ in keV}) .$$

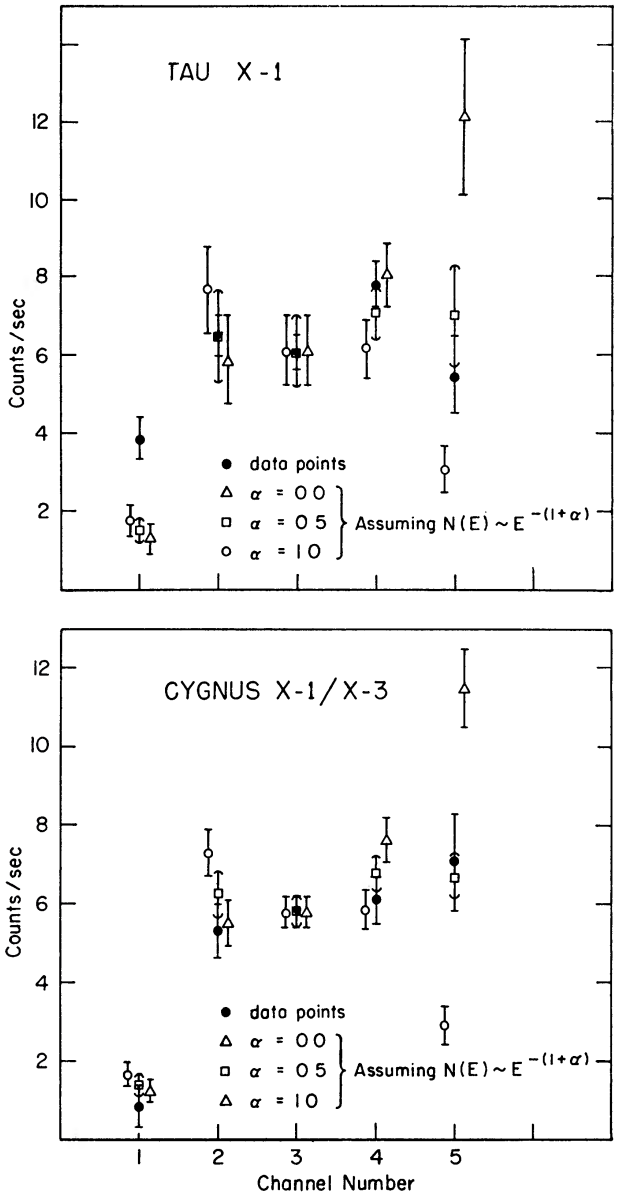

FIG 6.—Counting rates in the five channels for the Tau X-1 and Cygnus source(s) The solid circles are the observed rates. Under the assumption of a power-law spectrum the expected counting rates are given for three values of α To avoid confusion the $\alpha = 1\ 0$ data are presented somewhat to the left of channel numbers, the $\alpha = 0\ 0$ data somewhat to the right.

This relation was experimentally determined. Two incident spectra were assumed: one of the approximate form expected for X-ray emission from a hot, optically thin gas, namely,

$$N(E) = N_0 \left(\frac{E_0}{E}\right) e^{-E/kT},$$

and the other, a power law of the form

$$N(E) = N_0(E/E_0)^{-(1+\alpha)}.$$

The results obtained with the second spectrum are shown in Figure 6 for several values of the parameter α. Similar diagrams were made for the exponential spectrum. The error bars as presented are mainly due to energy channel setting uncertainties. From the in-flight energy calibration (every 10 min) we derived the channel boundaries for the Cygnus source: 9.8 ± 0.6, 19.7 ± 0.5, 34.0 ± 1.0, 47.4 ± 0.5, and 69.8 ± 1.2 keV. For the Tau X-1 source we found: 11.2 ± 1.0, 19.9 ± 0.5, 35.2 ± 2.0, 47.9 ± 0.8, 70.6 ± 1.5 keV.

The spectra of Tau X-1 and Cyg X-1/X-3 are evidently similar in shape and absolute intensity from 20 to 70 keV. However, the data from this experiment alone are not sufficiently accurate in either case to decide whether one or the other of the two spectral forms gives a significantly better fit. Under the exponential energy distribution assumption the data for both Tau X-1 and Cyg X-1/X-3 are consistent with values of kT from 40 to 80 keV. Under the power-law assumption the data are consistent with values of the optical index α from 0.4 to 0.8 for both sources.

In order to compare our data with other results on the spectra of these sources, we also derived estimates of the differential number spectra of the X-rays above the atmosphere in the three energy intervals corresponding to the differential pulse height intervals of channels 2, 3, and 4. (Channels 1 and 5 cannot be represented usefully this way.) For each of these channels we found the ratio between the integrated primary intensity in the given energy interval and the calculated counting rate, assuming a power law primary spectrum with $\alpha = 0.6$ and taking into account the effects of detector resolution and escape radiation. These ratios, which are, in fact, quite insensitive to the spectrum form, were assumed to be the factor by which our observed counting rates were to be multiplied to convert them into estimated points on the primary spectrum. The results are shown in Figure 7, together with some earlier results.

Of particular interest for future reference in the search for possible time variation is the ratio of the intensity of Cyg X-1/X-3 to that of Tau X-1. The present data give for this ratio the value of 0.84 ± 0.10 from 20 to 70 keV on July 19, 1966.

IV. DISCUSSION

a) Tau X-1

The earlier data of Clark (1965) have been reanalyzed taking iodine K X-ray escape (Stein and Lewin 1967) into account. (It was found that in the old analysis of channel 5 a factor 4 was overlooked so that the upper limit on the intensity for the energy channel > 62 keV should be increased by a factor of 4.) As shown in Figure 7, the spectrum values derived from the present data seem to be systematically lower, although the logarithmic slopes are in agreement within the rather large uncertainties in both sets of data. The present data agree reasonably well with those of Peterson *et al* (1966). The agreement would be improved if their results were corrected for the escape of iodine K X-rays. This correction would raise their value for the intensity at 35 keV by about 25 per cent and decrease it below the iodine K-edge at 32 keV. The high-energy ends of the rocket data of Grader *et al.* (1966) are also presented in Figure 7; they match well with the present data at 20 keV. No comparison is made with the data reported by

Haymes and Craddock (1966). We believe that the specific problem of background subtraction may have caused systematic errors in their analysis.

b) Cygnus

Our data demonstrate that Cyg X-2, recently identified as a variable blue starlike object (Giacconi, Gorenstein, Gursky, Usher, Waters, Sandage, Osmer, and Peach 1967) is less than one-eighth as bright as Cyg X-1 and Cyg X-3 combined in the energy range from 20–70 keV. This result is in disagreement with that of Brini *et al.* (1967), who concluded from their observations that Cyg X-2 was at least ten times brighter than Cyg

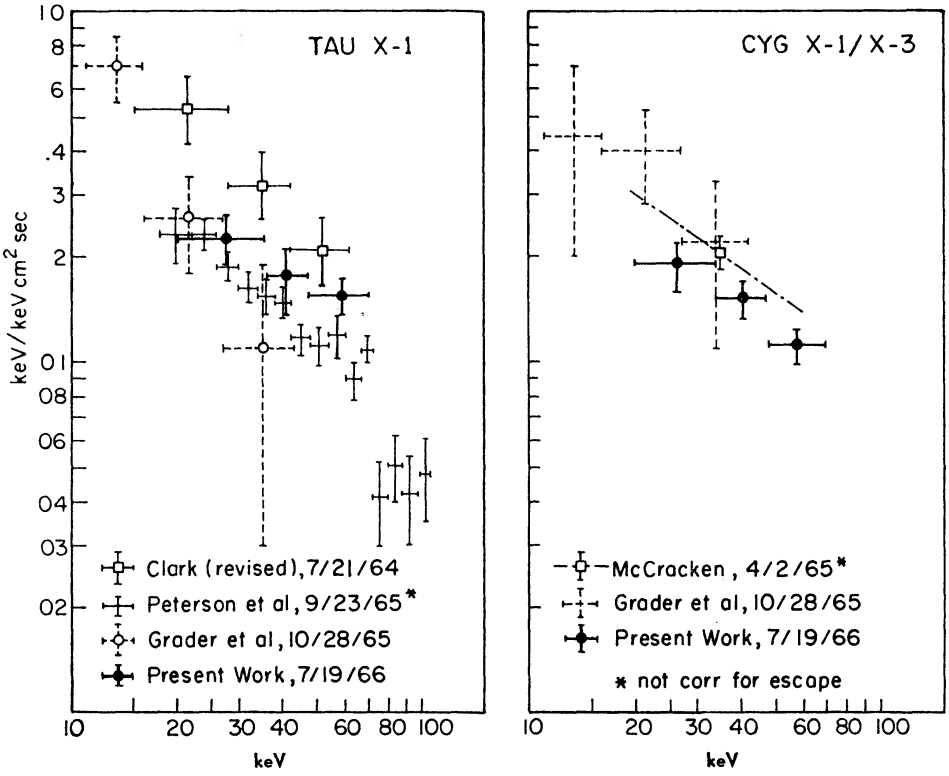

FIG. 7.—Energy spectra of Tau X-1 and Cygnus X-1/X-3

X-1/X-3. Since a relative intensity change of a factor of 80 seems very unlikely, it would appear that there was an error in their identification.

The rocket observations of Giacconi, Gorenstein, Gursky, and Waters (1967) showed that Cyg X-2 had an intensity comparable to the sum of Cyg X-1 and Cyg X-3 at 3 keV on October 11, 1966. Comparing their results with ours near 30 keV and assuming that the spectrum did not change between July and October, we conclude in agreement with McCracken (1966) that the spectrum of Cyg X-2 falls off much more rapidly than Cyg X-1/X-3 in the 3–30-keV energy range. In this way it appears to resemble the other identified variable blue starlike X-ray source, Sco X-1, which has also been observed to have a relatively soft spectrum compared to Tau X-1 and Cyg X-1/X-3.

Comparing our results on the Cyg X-1/X-3 source(s) with those of McCracken (1966) we find good agreement within the errors of measurements as indicated in Figure 7. A correction for iodine K escape X-rays would increase the intensity reported by McCracken at 35 keV by about 25 per cent, but would still preserve a reasonable agreement. There is also good agreement with the results obtained by Overbeck, Womack, and

Tananbaum (1967) in September, 1966. The data of Grader *et al.* have been presented to allow for a comparison with rocket results. Considering the uncertainties in the observations, we can set an upper limit of a factor of 1.5 on the intensity change of Cygnus X-1/X-3 between the date of McCracken's observation, April 2, 1965, and the date of the present data, July 19, 1966, in the energy range around 35 keV.

A recent flight on February 13, 1967, with the same instrument has surveyed the sky from right ascension 4^h to 23^h and declination $-23°$ to $+87°$. The results will be presented in a forthcoming paper.

We thank J. A. Stein and W. R. Scarlett for their assistance in conducting the experiment, and Mrs. T. Thorsos, R. Peterson, V. Leong, M. Gerassimenko, and Miss L. A. Wetherell for their help in computer programming and data analysis. We thank J. Overbeck for helpful discussions and for making available the results of his observations before publication. We also thank the staff of the Balloon Base of the National Center for Atmospheric Research for the successful flight operation.

REFERENCES

Bleeker, J. A. M., Burger, J. J., Deerenberg, A. J. M., Scheepmaker, A., Swanenburg, B. N., and Tanaka, Y. 1967, *Ap. J.*, **147**, 391.
Boldt, E., McDonald, F. B., Riegler, G., and Serlemitsos, P. 1966, *Phys. Rev. Letters*, **17**, 447.
Brini, D , Ciriegi, U., Fuligni, F., Moretti, E., and Vespignani, G. 1967 (preprint).
Clark, G. W. 1965, *Phys. Rev. Letters*, **14**, 91.
Giacconi, R., Gorenstein, P., Gursky, H., Usher, P. O., Waters, J. R., Sandage, A., Asmer, P., and Peach, J. V. 1967, *Ap. J.*, **148**, L129.
Giacconi, R., Gorenstein, P., Gursky, H., and Waters, J. R. 1967, *Ap. J.* (*Letters*), **149**, L85.
Grader, R. J., Hill, R. W., Seward, F. D , and Toor, A. 1966, *Science*, **152**, 1499.
Haymes, R. C., and Craddock, W. L. 1966, *J. Geophys. Res.*, **71**, 3261.
McCracken, K. G. 1966, *Science*, **154**, 1000.
Overbeck, J. W., Womack, E. A., and Tananbaum, H. D. 1967, *Ap. J.*, **150**, 47.
Peterson, L. E., and Jacobson, A. S. 1966, *Ap. J.*, **145**, 962.
Peterson, L. E., Jacobson, A. S., and Pelling, R. M. 1966, *Phys. Rev. Letters*, **16**, 142.
Rocchia, R., Rothenflug, R., Boclet, D., Ducros, G., and Labeyrie, J. 1966, *7th Internat. Space Sci. Symp., Vienna.*
Stein, J. A., and Lewin, W. H. G. 1967, *J. Geophys. Res.*, **72**, 383.